

Spontaneous Micro Flocking of Active Inertial Particles without Alignment Interaction

Subhajit Paul,^{1,2,*} Suman Majumder,^{3,†} and Wolfhard Janke^{4,‡}

¹*International Center for Theoretical Sciences, Tata Institute of Fundamental Research, Bangalore 560089, India*

²*Department of Physics and Astrophysics, University of Delhi, Delhi 110007, India*

³*Amity Institute of Applied Sciences, Amity University Uttar Pradesh, Noida 201313, India*

⁴*Institut für Theoretische Physik, Universität Leipzig, IPF 231101, 04081 Leipzig, Germany*

(Dated: February 8, 2024)

Observing spontaneous velocity ordering or flocking during motility induced phase separation (MIPS) in a system of spherical active Brownian particles without alignment interaction is challenging. We take up this problem by performing simulations of spherical active inertial particles with purely repulsive potential in presence of thermal noise and absence of any explicit alignment interaction. Our results not only show the presence of MIPS, but also reveal a micro-flocking transition. We characterize this transition in terms of a velocity order parameter as well as a characteristic length scale derived from the spatial correlation of the velocities.

PACS numbers: 05.70.Ln

Dynamics of many living objects, such as fishes, birds, bacteria, covering a wide range of length scale are modeled as “active” particles [1–23]. For them dissipation and consumption of energy happen at the level of single particle. On top of that, existence of self propulsion makes both single-particle behavior and their collective motion entirely different from passive particles [10, 11, 13–22]. Models with these characteristics invoked, on introduction of interaction among the particles make it an appropriate candidate to explore various nonequilibrium pattern formations and emergence of flocking in the real biological systems [3–6, 12, 16–19, 21, 22].

The minimal model of Vicsek *et al.* was the first to explore such a collective phenomenon [10]. For sufficiently high density and low thermal noise, in presence of a local velocity-alignment interaction among the particles, the model shows a transition from a disordered to an ordered state where particles move coherently forming a traveling band [13]. Motion of micro-organisms in a supposed to be viscous medium can be modeled using overdamped active Brownian particles (ABPs) [2, 5, 14, 16, 18, 24, 25]. Such a system of ABPs, even with a repulsive interaction and in absence of any alignment interaction among them shows clustering when the density is higher than a threshold value. This is formally known as motility induced phase separation (MIPS) [5, 14, 16, 18], resembling a vapor-liquid-like phase transition [26] or clustering in granular gas [27]. However, due to the stochastic nature of the propulsion direction, for spherical ABPs or similar non-polar particles, any kind of orientational or velocity ordering during MIPS is unlikely. For non-spherical particles, e.g., dumbbells, rods, elongated micro swimmers, where the microscopic isotropy is broken, one observes velocity ordering even in absence of any explicit alignment interaction among them [28–33]. Velocity ordering has been observed for spherical particles in presence of explicit alignment interaction and with repulsive interaction [34, 35]. Recently, it has also been observed even in absence of explicit alignment

interaction with only repulsive interaction among the ABPs, however, in absence of any thermal noise and very high packing fraction [36].

In most of the studies on ABPs in the past, the dynamics was considered to be overdamped. This is motivated by the very small sizes (between nm to μm) of real systems, viz., colloids or micro-organisms, which they are thought to be representing, and hence the inertial effect can be neglected in comparison to the drag force of the solvent. However, this approximation does not stand as a general approach. Especially, when active particles are supposed to change velocities during their motion [37, 38]. Interestingly, inclusion of the inertial effect changes the MIPS behavior drastically. In such a scenario, it has been shown that for sufficiently large self-propulsion force, MIPS becomes reentrant [39]. To observe MIPS, particles in the high density region are supposed to move slowly leading to an eventual formation of clusters. For an overdamped particle, this is possible due to slowing down of overdamped particles following a collision. However, underdamped particles can bounce back from collision without slowing down until it encounters the next collision. Hence, at large self-propulsion velocity one observes a breakdown of the MIPS.

In this context, a recent study of underdamped spherical ABP with attractive interaction observed “flocking” or orientational ordering without any explicit alignment interaction [40]. There it has been argued that the effective alignment interaction between the particles results from the interplay between persistent active forces and attractive interactions, which gets manifested as a flocking transition. In this Letter, we take a step ahead and show that “flocking” can be observed for spherical underdamped active particles, i.e., active inertial particles (AIP) in absence of any explicit alignment interaction even without attractive interactions, that is with a completely repulsive interaction only.

We consider N interacting spherical AIPs in space dimension $d = 2$. Equations governing their translational and rota-

* spaul@physics.du.ac.in, subhajitphys@gmail.com

† suman.jdv@gmail.com

‡ wolfhard.janke@itp.uni-leipzig.de

tional motions are [8, 41]

$$m_i \frac{d^2 \vec{r}_i}{dt^2} = -\gamma_t \frac{d\vec{r}_i}{dt} - \vec{\nabla} U_i + \vec{f}_i^a + \sqrt{2\gamma_t k_B T} \vec{\xi}_i(t), \quad (1)$$

$$\gamma_r \frac{d\theta_i}{dt} = \sqrt{2\gamma_r k_B T} \eta_i(t). \quad (2)$$

Here $m_i = m$ is the mass of the i -th particle, \vec{r}_i represents its position and θ_i is the propulsion direction. γ_t and γ_r represent the translational and rotational drag coefficients, respectively, and T is the temperature. The Gaussian white noises $\vec{\xi}_i$ and η_i have zero mean and unit variance, and are Delta-correlated over space and time. The passive interaction U_i as a function of the inter-particle distance r is modeled by the repulsive Weeks-Chandler-Andersen potential [42] $V_{WCA}(r) = 4\epsilon[(\sigma/r)^{12} - (\sigma/r)^6] + 1/4$, with $r < 2^{1/6}\sigma$ and 0 otherwise. We set both diameter of the particles σ and the interaction strength ϵ to unity. The active force for the i -th particle is defined by $\vec{f}_i^a = f^a \hat{n}_i$, where f^a and $\hat{n}_i \equiv (\cos \theta_i, \sin \theta_i)$ represent, respectively, the strength and the direction of activity or self propulsion. The translational and rotational diffusion coefficients are given as $D_{t,r} = k_B T / \gamma_{t,r}$. Here, we keep the ratio $D_t/D_r = \sigma^2/3$ fixed with $\gamma_t = 5.0$. In this context, there are two time scales, viz., the persistence time $\tau_p = 1/D_r$ defining the characteristic time after which the propulsion direction of a particle alters and the inertial time $\tau_m = m/\gamma_t$ representing the time required for a particle to achieve its terminal speed. As a measure of inertia of the particles, we define a parameter $\kappa = \tau_m/\tau_p (= mD_r/\gamma_t)$, which is varied by changing m . Unless otherwise mentioned, we simulate a system with a packing fraction $\phi = N\pi\sigma^2/(4L^2) = 0.39$ at $T = 0.1$ in a square box of linear dimension $L = 128$ with periodic boundary condition in both directions. We apply the velocity-Verlet algorithm to integrate the equation of motions [43], where the time step is chosen to be 0.01 in units of $\tau_0 = \gamma_t \sigma^2/\epsilon$. In the rest of the paper activity is expressed in terms of the dimensionless Péclet number $Pe = f^a \sigma / k_B T$, the ratio between the active energy $f^a \sigma$ and thermal energy $k_B T$ [4, 8]. Unless otherwise mentioned, the subsequent results presented are for $Pe = 150$.

We start by showing in Fig. 1 representative snapshots of steady-state configurations which are obtained by starting from a random initial condition and letting the simulations run for a considerable amount of time until they reach a steady state. The chosen values of κ in Figs. 1(a)-(d) correspond to masses $m = 10^{-2}, 10^{-1}, 1.0$, and 10.0. The snapshots in Figs. 1(a)-(c) clearly show phase separation between low- and high-density phases, reminiscent of the vapor-liquid phase separation in a system of passive particles with attractive interactions [26]. However, here the phase separation is solely driven by the activity in presence of a repulsive interaction among the particles, hence, basically it is an MIPS. Interestingly, in this case, unlike for ABPs, no phase separation is observed for higher values of κ , evident from the snapshot presented in Fig. 1(d).

For a quantitative understanding of the above mentioned MIPS, in Figs. 1(a)-(d) we also show the plots of normalized distributions $P(\rho_{loc})$ of the local densities ρ_{loc} for different values of the inertia parameter κ . To calculate ρ_{loc} , at first

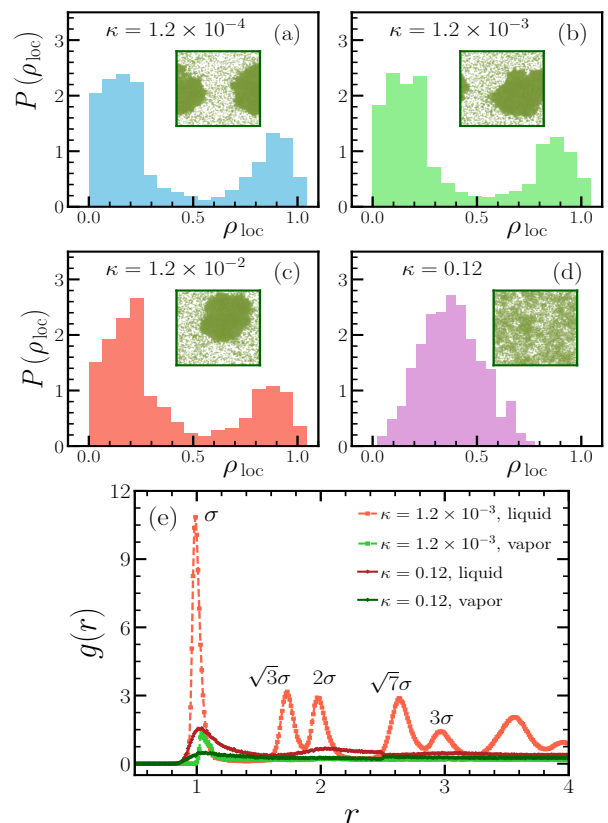


FIG. 1. (a)-(d) Normalized distributions $P(\rho_{loc})$ of the local density ρ_{loc} for steady-state configurations at different values of the inertial parameter κ . Representatives of corresponding configurations are also shown. (e) Radial distribution function $g(r)$ considering separately the particles within the “liquid” and “vapor” phases for different values of κ .

we divide the whole simulation box into a number of smaller square boxes, each of size $4\sigma \times 4\sigma$. Then, the particle density ρ_{loc} of each of these spatially distributed boxes is calculated. For Figs. 1(a) and (b), i.e., for the lower values of κ , two peaks appear at $\rho_{loc} \approx 0.15$ and ≈ 0.9 , corresponding to the densities of the “vapor”-like and “liquid”-like phases, respectively. With increasing κ the separation between the peaks gradually decreases [Fig. 1(c)]. For $\kappa = 0.12$ the distribution becomes single peaked around $\rho_{loc} \approx 0.39$ indicating a homogeneous distribution of the particles [Fig. 1(d)]. We have checked roughly that MIPS does not occur for $\kappa > 0.05$. Thus, for the rest of the Letter, for MIPS we choose κ according to this limiting value.

To have an understanding of the structure formation of the observed MIPS, we calculate the radial distribution function $g(r) = n(r)/(2\pi r \delta r)$, where $n(r)$ counts the number of particles within a shell of width δr . In Fig. 1(e) we show plots of $g(r)$ separately for “vapor” and “liquid” phases for two different values of κ . For $\kappa = 1.2 \times 10^{-3}$, in the liquid-like phase, one sees different peaks, well separated from each other. The peaks appearing at $1, \sqrt{3}, 2, \sqrt{7}, 3, \dots$ in units of σ suggest a hexagonal quasi-periodic arrangement of the particles. Also, finite values of $g(r)$ for $r < \sigma$ indicate inter-particle

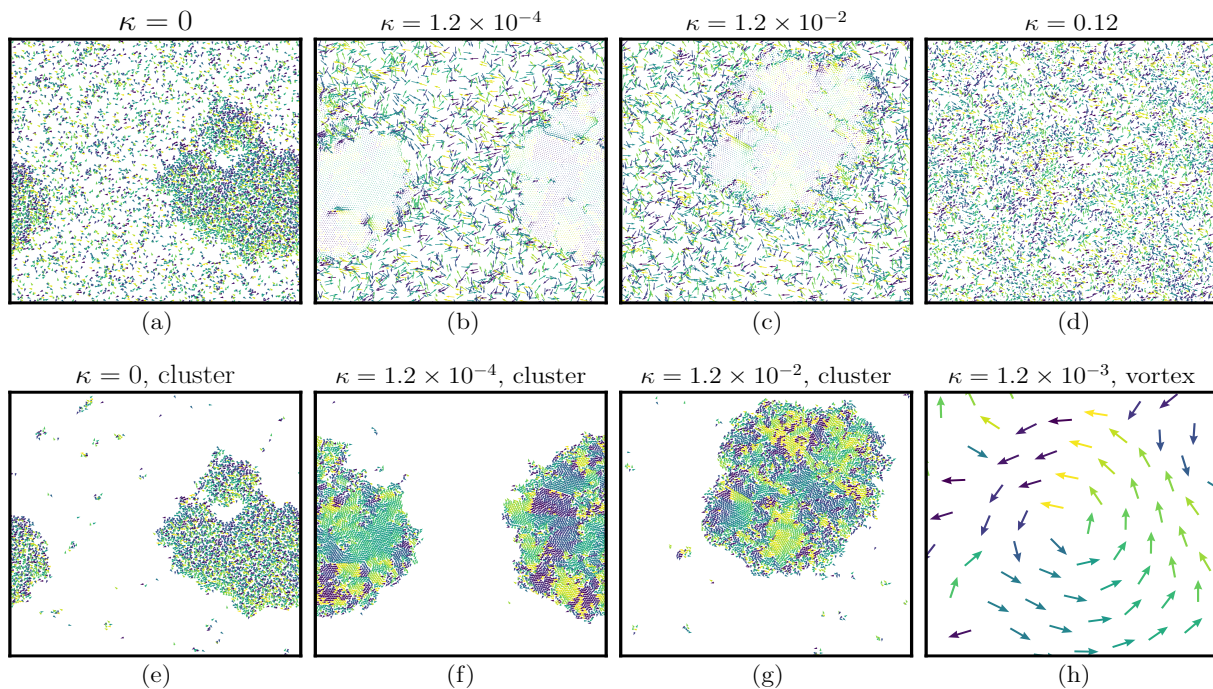


FIG. 2. (a)-(d) Typical velocity fields of all the particles for different values of κ . (e)-(g) Velocities of the particles only within the clustered region for $\kappa = 0, 1.2 \times 10^{-4}$ and 1.2×10^{-2} . (h) Section of a cluster showing a typical vortex-like defect for $\kappa = 1.2 \times 10^{-3}$.

separations smaller than σ which in turn implies the existence of an effective attraction between the particles in the liquid-like phase. Since only a repulsive force is acting between the particles, it can be inferred that the effective attraction arises owing to the activity or self propulsion [44]. On the other hand, for the “vapor” phase we see only one peak with much lower height followed by a constant value of $g(r)$ close to 0. This indicates random arrangements of the particles in the

“vapor” region. We also plot $g(r)$ for $\kappa = 0.12$ where no MIPS is observed. There, the “liquid” and “vapor” correspond to particles having a local density ρ_{loc} higher and lower than the threshold value $\rho_c = 0.5$, respectively. Since the system is almost homogeneous, for both of them we observe only a single peak near $r \approx \sigma$ followed by a flat region, and the difference in the peak heights is insignificant compared to the case of $\kappa = 1.2 \times 10^{-3}$.

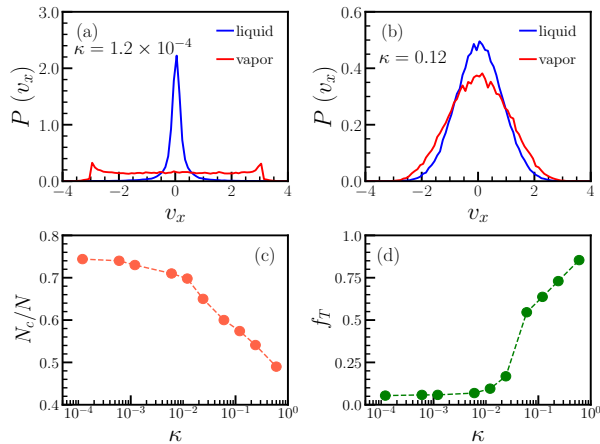


FIG. 3. (a)-(b) Distributions of the x -component of velocity $P(v_x)$ of particles for high and low density regions, marked as “liquid” and “vapor”, respectively, for two different κ . (c) Fraction of particles that are part of any cluster as a function of κ . (d) Ratio f_T between kinetic temperatures of the “liquid” and “vapor” regions versus κ . Error bars in (c) and (d) are of the size of the data points.

Moving on to our primary interest, in Figs. 2(a)-(d) we show the velocity field of the particles for increasing κ . For $\kappa = 0$ we consider the components of the vectors provided by θ_i as $(f^a \cos \theta_i, f^a \sin \theta_i)$ whereas for $\kappa > 0$ we show the velocity components (v_i^x, v_i^y) . For $\kappa = 0$, the particles within or outside the cluster move with same magnitude of velocity f^a . Now for $\kappa > 0$, but with lower values, as observed from Figs. 2(b) and (c), interestingly, the particles within the cluster have much lower velocities compared to the ones outside. For even a higher value of $\kappa = 0.12$, as shown in Fig. 2(d), where there is no MIPS the velocities of all the particles are also uniform. In Figs. 2(e)-(g) we show the velocities of only the clustered particles, for $\kappa = 0, 1.2 \times 10^{-4}$ and 1.2×10^{-2} , respectively. There, for a better visualization, we fixed the magnitude of the velocity vector of each particle to unity. Different colors represent distinct directional angles ranging from $-\pi$ to π . With these one clearly observes the coexistence of different domains where the particle velocities are ordered. The number of domains is larger and the fluctuations near the boundaries are higher for $\kappa = 1.2 \times 10^{-2}$, suggesting lower degree of alignment for higher κ . This we will quantify later by calculating the correlation length and a suitable Vicsek-like order parameter. Finally, in Fig. 2(h) we show the presence of

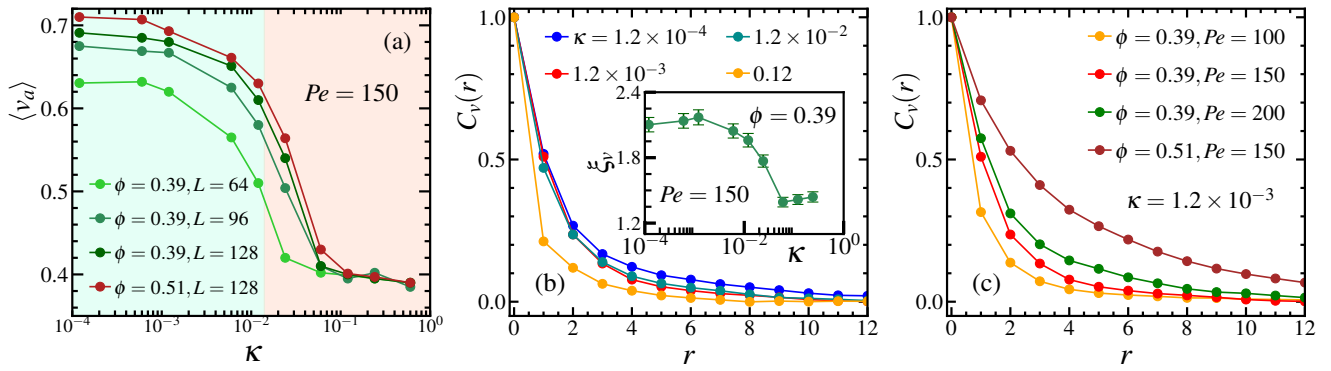


FIG. 4. (a) Velocity order parameter $\langle v_a \rangle$ versus the inertia parameter κ for different choices of the packing fraction ϕ and system size L . Different colored regions are guide to eye. (b) Normalized velocity correlation $C_v(r)$ for different values of κ for $\phi = 0.39$ and $Pe = 150$. Inset shows the variation of the correlation length $\xi_v = \int C_v(r) dr$ vs κ . (c) shows $C_v(r)$ for different choices of ϕ and the activity parameter Pe for a fixed $\kappa = 1.2 \times 10^{-3}$.

vortex-like defects at the boundaries of differently ordered domains for $\kappa = 1.2 \times 10^{-3}$. Thus, for a certain intermediate range of the inertial parameter κ , flocking of particles within micro domains appear. From the plots of $g(r)$ in Fig. 1(e) we already get a hint that the interparticle separation r can be less than σ , indicating an effective attraction even in presence of a purely repulsive interaction. This possibly helps in developing correlated velocities among neighboring particles within the clusters.

Like the differences in the density field, there exist significant differences in velocities as well while considering particles within and outside the cluster. This is evident from the normalized distributions $P(v_x)$ of the x -component of the velocity plotted in Figs. 3(a) and (b), respectively, for $\kappa = 1.2 \times 10^{-4}$ and 0.12. Like in Fig. 1(e), here also we present two different data sets corresponding to the distributions of the particles in “liquid” and “vapor” regions, i.e., for clustered and non-clustered regions. For $\kappa = 1.2 \times 10^{-4}$, the non-clustered “vapor” particles show almost a flat distribution, while the one for the clustered particles appears to be single-peaked near $v_x \approx 0$. However, for $\kappa = 0.12$ as there is no MIPS, the distributions $P(v_x)$ for both the so-called “vapor” and “liquid” seem to be normal distributions, expected for a homogeneous system. To check what fraction of the total number of particles becomes part of the “liquid” region or the cluster, for different values of κ , in Fig. 3(c) we plot the fraction N_c/N versus κ , where N_c is the number of particles that are part of any cluster. We see that for $\kappa < 1.2 \times 10^{-2}$ this number is ≈ 0.75 . Then with increasing κ , N_c/N decreases and for $\kappa > 6.0 \times 10^{-2}$ this fraction tends towards ≈ 0.45 when there is no MIPS.

Even though we find only micro domains of ordered velocities, the distributions in Fig. 3(a) prompted us to calculate the effective temperatures defined from the corresponding average kinetic energy as

$$T_{\text{eff}}^{l,v} = \frac{m}{2k_B} \left[\langle v_x^2 \rangle + \langle v_y^2 \rangle \right]_{l,v}, \quad (3)$$

where T_{eff}^l and T_{eff}^v are, respectively, the effective tempera-

tures of the “liquid” and “vapor” regions, and $\langle \dots \rangle$ represents average over particles in those regions. In Fig. 3(d) we plot the ratio $f_T = T_{\text{eff}}^l / T_{\text{eff}}^v$ as function of κ . We see that f_T increases monotonically from ≈ 0.5 toward 1 with increasing κ . While a small value of f_T indicates significant difference in the effective temperatures of the “liquid”-like and “vapor”-like regions, f_T approaching unity indicates that the difference becomes negligible. f_T shows a jump around $\kappa \approx 0.05$ which nicely coincides with the value above which MIPS does not appear.

To understand the local velocity ordering we define a Vicsek-like order parameter, related to the orientation of the particles as [10, 45]

$$v_a = \frac{1}{N_c} \sum_{i=1}^{N_c} \frac{\left| \sum_{k=1}^{n_i} \vec{v}_k^i \right|}{\sum_{k=1}^{n_i} |\vec{v}_k^i|}. \quad (4)$$

In Eq. (4) the summation runs over all N_c particles which are part of a cluster. For each of this particle i , n_i denotes the number of particles that are within a distance $r_c = 2.5\sigma$ from it. Even though the velocities are not globally aligned in the clustered region, the order parameter v_a is sufficient to capture the formation of micro domains of ordered velocities. This is demonstrated in Fig. 4(a) where we present the variation of $\langle v_a \rangle$ as function of the inertial parameter κ for different packing fractions ϕ and lattice sizes L . There $\langle \dots \rangle$ denotes a steady-state average over different micro clusters and initial realizations. It clearly reflects a micro-flocking transition which becomes more prominent as L increases. Of course, an increase in the particle density also sharpens the transition as shown by the data for $\phi = 0.51$ for $L = 128$. The different colored regions are somewhat a guide to the eye as the system moves from a velocity ordered state to a state with random velocity ordering with increasing κ .

To further substantiate the micro-flocking transition in terms of a length scale, we calculate the two-point velocity-velocity correlation function

$$C_v(r) = \frac{\langle \vec{v}_i \cdot \vec{v}_j \rangle - \langle \vec{v}_i \rangle \cdot \langle \vec{v}_j \rangle}{\langle v_i^2 \rangle - \langle v_i \rangle^2}, \quad (5)$$

where $r = |\vec{r}_i - \vec{r}_j|$ is the scalar distance between particles i and j . In Fig. 4(b) we plot $C_v(r)$ for different values of κ in the steady states. For smaller κ where MIPS exists, we consider particles that are part of the “liquid” phase, whereas for larger κ all the particles of the system are taken into account. Faster decay of $C_v(r)$ with increasing κ clearly indicates the presence of a growing length scale capturing the micro-flocking transition. As a quantitative estimation we measure the correlation length $\xi_v = \int C_v(r) dr$ and show its variation as a function of κ in the inset of Fig. 4(b). The behavior is very similar to what is observed for $\langle v_a \rangle$ in Fig. 4(a), indicating the micro-flocking transition as a function of κ .

To understand the effect of packing fraction and activity strength on the velocity ordering, in Fig. 4(c) we plot $C_v(r)$ for different combinations of Pe and ϕ for $\kappa = 1.2 \times 10^{-3}$. The slower decay of $C_v(r)$ with increasing activity as well as with packing fraction indicates higher range of velocity ordering of the particles within the micro domains. A detailed quantification of $\langle v_a \rangle$ and ξ_v for a complete understanding of the observed micro flocking with variation of ϕ and Pe will be presented elsewhere.

In conclusion, we have reported the first observation of micro-flocking behavior in a system of purely repulsive AIPs in presence of thermal noise but absence of any explicit alignment interaction. Previously, in Ref. [40] in presence of attractive interactions a flocking transition with AIPs has been observed, which was conjectured to be an outcome of the interplay of the attractive force with the strong persistence motion at high activities. Thus, our results challenge the generality of this conjecture and rather indicate that flocking is observed due to an effective attraction among the AIPs solely caused by the presence of strong self-propulsion forces [44].

Our findings are relevant for any macroscopic living objects where inertial effects cannot be ignored. For small values of κ , the observed MIPS (for the density phase separation) is similar to what is expected for overdamped ABPs. However, interestingly, within the “liquid” phase, there appear vast differences in the velocity field with emergence of micro domains within which the velocities of AIPs are locally ordered. Also,

the effective temperatures of the “liquid” and “vapor” regions appear to be different, unlike for an ABP system. For much larger κ , the MIPS behavior is no more observed, and thereby the micro-flocking transition also disappears. We have shown that the variations of the velocity order parameter and correlation length, with respect to κ , can be used as quantitative probes for this micro-flocking transition. Overall, our results establish the fact that micro-flocking of particles is rather a generic phenomenon. Thus it will be interesting to look at the interplay between the effects of Pe and κ on such velocity ordering. As a future work, we plan to study the steady-state phase diagram in this regard.

In future, it will also be interesting to study the nonequilibrium scaling laws [46] associated with such velocity ordering of AIPs and the role of defect annihilation. Definitely, the effect of increasing activity and packing fraction on exchanging information among the particles, as suggested in Fig. 4(c), is also worth to investigate. Another future endeavour would be to investigate the dynamics of such a system exploring various transport properties. Considering the recent interests in the behavior of active polymers in general [4, 25, 45, 47–49], it would also be intriguing to study the structure and dynamics of a polymer consisting of AIPs as monomers.

ACKNOWLEDGMENTS

S.P. thanks Debasish Chaudhuri for useful discussions and acknowledges ICTS-TIFR, DAE, Govt. of India for a research fellowship. This work was funded by the Deutsche Forschungsgemeinschaft (DFG, German Research Foundation) under Grant No. 189 853 844 – SFB/TRR 102 (Project B04) and further supported by the Deutsch-Französische Hochschule (DFH-UFA) through the Doctoral College “ \mathbb{L}^4 ” under Grant No. CDFA-02-07, and the Leipzig Graduate School of Natural Sciences “BuildMoNa”. S.M. thanks the Science and Engineering Research Board (SERB), Govt. of India for funding through a Ramanujan Fellowship (file no. RJF/2021/000044).

-
- [1] H. Chaté, F. Ginelli, G. Grégoire, F. Peruani, and F. Raynaud, Modeling collective motion: Variations on the Vicsek model, *Eur. Phys. J. B* **64**, 451 (2008).
 - [2] P. Romanczuk, M. Bär, W. Ebeling, B. Lindner, and L. Schimansky-G., Active Brownian particles, *Eur. Phys. J. Spec. Top.* **202**, 1 (2012).
 - [3] M. C. Marchetti, J. F. Joanny, S. Ramaswamy, T. B. Liverpool, J. Prost, M. Rao, and R. A. Simha, Hydrodynamics of soft active matter, *Rev. Mod. Phys.* **85**, 1143 (2013).
 - [4] J. Elgeti, R. G. Winkler, and G. Gompper, Physics of microswimmers—single particle motion and collective behavior: A review, *Rep. Prog. Phys.* **78**, 056601 (2015).
 - [5] M. E. Cates and J. Tailleur, Motility-induced phase separation, *Ann. Rev. Cond. Mat. Phys.* **6**, 219 (2015).
 - [6] C. Bechinger, R. Di Leonardo, H. Löwen, C. Reichhardt, G. Volpe, and G. Volpe, Active particles in complex and crowded environments, *Rev. Mod. Phys.* **88**, 045006 (2016).
 - [7] M. R. Shaebani, A. Wysocki, R. G. Winkler, G. Gompper, and H. Rieger, Computational models for active matter, *Nat. Rev. Phys.* **2**, 181 (2020).
 - [8] H. Löwen, Inertial effects of self-propelled particles: From active Brownian to active Langevin motion, *J. Chem. Phys.* **152**, 040901 (2020).
 - [9] L. Caprini and U. M. B. Marconi, Inertial self-propelled particles, *J. Chem. Phys.* **154**, 024902 (2021).
 - [10] T. Vicsek, A. Czirók, E. Ben-Jacob, I. Cohen, and O. Shochet, Novel Type of Phase Transition in a System of Self-Driven Particles, *Phys. Rev. Lett.* **75**, 1226 (1995).
 - [11] G. Grégoire and H. Chaté, Onset of Collective and Cohesive Motion, *Phys. Rev. Lett.* **92**, 025702 (2004).
 - [12] A. Sokolov, I. S. Aranson, J. O. Kessler, and R. E. Goldstein, Concentration Dependence of the Collective Dynamics of Swimming Bacteria, *Phys. Rev. Lett.* **98**, 158102 (2007).

- [13] H. Chaté, F. Ginelli, G. Grégoire, and F. Raynaud, Collective motion of self-propelled particles interacting without cohesion, *Phys. Rev. E* **77**, 046113 (2008).
- [14] S. Mishra, A. Baskaran, and M. C. Marchetti, Fluctuations and pattern formation in self-propelled particles, *Phys. Rev. E* **81**, 061916 (2010).
- [15] B. ten Hagen, S. van Teeffelen, and H. Löwen, Brownian motion of a self-propelled particle, *J. Phys.: Cond. Mat.* **23**, 194119 (2011).
- [16] Y. Fily and M. C. Marchetti, Athermal Phase Separation of Self-Propelled Particles with No Alignment, *Phys. Rev. Lett.* **108**, 235702 (2012).
- [17] J. Bialké, T. Speck, and H. Löwen, Crystallization in a Dense Suspension of Self-Propelled Particles, *Phys. Rev. Lett.* **108**, 168301 (2012).
- [18] G. S. Redner, M. F. Hagan, and A. Baskaran, Structure and Dynamics of a Phase-Separating Active Colloidal Fluid, *Phys. Rev. Lett.* **110**, 055701 (2013).
- [19] S. K. Das, Pattern, growth, and aging in aggregation kinetics of a Vicsek-like active matter model, *J. Chem. Phys.* **146**, 044902 (2017).
- [20] A. Dhar, A. Kundu, S. N. Majumdar, S. Sabhapandit, and G. Schehr, Run-and-tumble particle in one-dimensional confining potentials: Steady-state, relaxation, and first-passage properties, *Phys. Rev. E* **99**, 032132 (2019).
- [21] S. Mandal, B. Liebchen, and H. Löwen, Motility-Induced Temperature Difference in Coexisting Phases, *Phys. Rev. Lett.* **123**, 228001 (2019).
- [22] S. Paul, A. Bera, and S. K. Das, How do clusters in phase-separating active matter systems grow? A study for Vicsek activity in systems undergoing vapor-solid transition, *Soft Matter* **17**, 645 (2021).
- [23] A. Bera, S. Sahoo, S. Thakur, and S. K. Das, Active particles in explicit solvent: Dynamics of clustering for alignment interaction, *Phys. Rev. E* **105**, 014606 (2022).
- [24] P. Digregorio, D. Levis, A. Suma, L. F. Cugliandolo, G. Gonnella, and I. Pagonabarraga, Full Phase Diagram of Active Brownian Disks: From Melting to Motility-Induced Phase Separation, *Phys. Rev. Lett.* **121**, 098003 (2018).
- [25] S. Paul, S. Majumder, and W. Janke, Activity mediated globule to coil transition of a flexible polymer in a poor solvent, *Soft Matter* **18**, 6392 (2022).
- [26] S. Majumder and S. K. Das, Universality in fluid domain coarsening: The case of vapor-liquid transition, *Europhys. Lett.* **95**, 46002 (2011).
- [27] S. Paul and S. K. Das, Dynamics of clustering in freely cooling granular fluid, *Europhys. Lett.* **108**, 66001 (2014).
- [28] I. S. Aranson and L. S. Tsimring, Model of coarsening and vortex formation in vibrated granular rods, *Phys. Rev. E* **67**, 021305 (2003).
- [29] F. Peruani, A. Deutsch, and M. Bär, Nonequilibrium clustering of self-propelled rods, *Phys. Rev. E* **74**, 030904 (2006).
- [30] F. Ginelli, F. Peruani, M. Bär, and H. Chaté, Large-scale Collective Properties of Self-Propelled Rods, *Phys. Rev. Lett.* **104**, 184502 (2010).
- [31] J. Deseigne, O. Dauchot, and H. Chaté, Collective Motion of Vibrated Polar Disks, *Phys. Rev. Lett.* **105**, 098001 (2010).
- [32] G. Briand and O. Dauchot, Crystallization of Self-propelled Hard Discs, *Phys. Rev. Lett.* **117**, 098004 (2016).
- [33] B. Bhattacharjee and D. Chaudhuri, Re-entrant phase separation in nematically aligning active polar particles, *Soft Matter* **15**, 8483 (2019).
- [34] K.-D. N. T. Lam, M. Schindler, and O. Dauchot, Self-propelled hard disks: Implicit alignment and transition to collective motion, *New J. Phys.* **17**, 113056 (2015).
- [35] E. Sesé-Sansa, D. Levis, and I. Pagonabarraga, Phase separation of self-propelled disks with ferromagnetic and nematic alignment, *Phys. Rev. E* **104**, 054611 (2021).
- [36] L. Caprini, U. M. B. Marconi, and A. Puglisi, Spontaneous Velocity Alignment in Motility-Induced Phase Separation, *Phys. Rev. Lett.* **124**, 078001 (2020).
- [37] A. Brown and W. Poon, Ionic effects in self-propelled pt-coated Janus swimmers, *Soft Matter* **10**, 4016 (2014).
- [38] C. Scholz, S. Jahanshahi, A. Ldov, and H. Löwen, Inertial delay of self-propelled particles, *Nat. Comm.* **9**, 1 (2018).
- [39] A. Suma, G. Gonnella, D. Marenduzzo, and E. Orlandini, Motility-induced phase separation in an active dumbbell fluid, *Europhys. Lett.* **108**, 56004 (2014).
- [40] L. Caprini and H. Löwen, Flocking Without Alignment Interactions in Attractive Active Brownian Particles, *Phys. Rev. Lett.* **130**, 148202 (2023).
- [41] C. Dai, I. R. Bruss, and S. C. Glotzer, Phase separation and state oscillation of active inertial particles, *Soft Matter* **16**, 2847 (2020).
- [42] J. D. Weeks, D. Chandler, and H. C. Andersen, Role of repulsive forces in determining the equilibrium structure of simple liquids, *J. Chem. Phys.* **54**, 5237 (1971).
- [43] D. Frenkel and B. Smit, *Understanding Molecular Simulation: From Algorithms to Applications* (Academic Press, San Diego, 2002).
- [44] A. Das, A. Dhar, and A. Kundu, Gap statistics of two interacting run and tumble particles in one dimension, *J. Phys A: Math. and Theo.* **53**, 345003 (2020).
- [45] S. Paul, S. Majumder, S. K. Das, and W. Janke, Effects of alignment activity on the collapse kinetics of a flexible polymer, *Soft Matter* **18**, 1978 (2022).
- [46] S. Majumder, H. Christiansen, and W. Janke, Understanding nonequilibrium scaling laws governing collapse of a polymer, *Eur. Phys. J. B* **93**, 142 (2020).
- [47] R. G. Winkler and G. Gompper, The physics of active polymers and filaments, *J. Chem. Phys.* **153**, 040901 (2020).
- [48] S. Paul, S. Majumder, and W. Janke, Motion of a polymer globule with Vicsek-like activity: From super-diffusive to ballistic behavior, *Soft Mater.* **19**, 306 (2021).
- [49] S. Majumder, S. Paul, and W. Janke, Activity induced enhanced diffusion of a polymer in poor solvent, arXiv preprint arXiv:2308.13856 (2023).